PAPER • **OPEN ACCESS**

Exploring small-angle in-plane oscillations of a rigid pendulum suspended from two points: theory and experiment

To cite this article: Stefano Oss 2025 *Phys. Educ.* **60** 045033

OPEN ACCESS

PAPER

Phys. Educ. **60** (2025) 045033 (7pp)

iopscience.org/ped

Exploring small-angle in-plane oscillations of a rigid pendulum suspended from two points: theory and experiment

Stefano Oss

Physics Department, University of Trento, 38123 Povo (Trento), Italy

E-mail: stefano.oss@unitn.it

CrossMark

Abstract
This study provides an introductory investigation into the oscillatory dynamics of a rigid bar suspended at both ends by two identical, inextensible strings attached to an adjustable horizontal support. Unlike the typical bifilar pendulum—which undergoes torsional motion—this system oscillates within its own plane, combining translational and rotational motion depending on the geometry of the suspension points. A simple theoretical Newtonian model is developed using the small-angle approximation, allowing predictions of the oscillation period and trajectories of the bar's endpoints. Experimental validation is performed using slow-motion video analysis and tracking software. The results show good agreement between theoretical predictions and experimental observations, highlighting the educational relevance of this system for undergraduate physics students and high school teachers. The setup effectively illustrates constrained rigid body motion and the associated oscillatory and roto-translational behaviours.

Keywords: classical mechanics, physical pendulum, small angle approximation,
rigid body oscillation

1. Introduction

The simple pendulum is a cornerstone of physics education [1], but its conceptual extensions offer opportunities to explore more advanced mechanical principles [2]. Rigid bar bifilar pendulums suspended by two identical strings, forming a two-point planar suspension, are interesting systems in which one can observe both torsional motion about a vertical axis [3, 4], and oscillations in the same plane as the bar [5]. In this work, we focus on the latter: we show how, by adjusting the distance between the suspension points on the support, the system transitions from a configuration where the bar rotates about a single fixed pivot (when the two suspension points coincide) to configurations where the bar's centre of mass undergoes translational motion in addition to rotation. These features make the system ideal for demonstrating constrained motion and for highlighting the role of geometry in dynamical behaviour.

Moreover, from a pedagogical standpoint, constructing a Newtonian model under the small-angle approximation offers significant educational benefits. Such an approach not only reinforces students' understanding of linearisation techniques but also enhances their appreciation of the powerful simplifications achievable through analytical approximations. Revisiting and reevaluating classical mechanical systems, such as the one presented here, can foster deeper conceptual insights into fundamental physical principles and methodological rigor. Indeed, the ability to systematically build and analyse simplified mechanical models remains a crucial skill for students, bridging theoretical physics with practical experimentation.

We derive a simple Newtonian theoretical model in the small-angle regime and validate it experimentally through the analysis of slow-motion video tracking. The setup relies on widely available tools, making the experiment easily replicable in educational settings—from high school teaching environments to undergraduate physics laboratories and classical mechanics courses.

2. Theoretical model

We outline here the model used to describe the double-suspended pendulum. It stems from a straightforward application of classical Newtonian mechanics, which can, of course, be found in any introductory college-level textbook [6, 7], as well as in similar case studies where the bifilar pendulum is considered to some extent [8]. The bar has length $2l$, and the suspension wires—of equal length l—are fixed to a horizontal ceiling at a distance $2d$ between them. The first step in this model is geometrical: the system has a single degree of freedom, which must be clearly identified. The wires are assumed to remain taut at all times, constraining the deformation of the quadrilateral formed by the bar, the wires, and the segment connecting the suspension points to the configuration shown in figure 1. A Cartesian reference frame Oxy is introduced with origin at the midpoint of the bar in its horizontal equilibrium position. Denoting (x_G,y_G) as the coordinates of the bar's midpoint G (i.e. the centre of mass), and introducing the angle θ between the bar and the horizontal, the coordinates of the endpoints A and B are:

$$\begin{aligned} \vec{r}_A &\equiv (x_G - L\cos\theta, y_G - L\sin\theta), \\ \vec{r}_B &\equiv (x_G + L\cos\theta, y_G + L\sin\theta). \end{aligned} \tag{1}$$

The suspension points A_0 and B_0 are located at

$$\vec{r}_{A_0} \equiv (-d, h), \vec{r}_{B_0} \equiv (+d, h) \tag{2}$$

where $h = \sqrt{l^2 - (L-d)^2}$ is the vertical distance of the bar from the ceiling. This distance requires, of course, that the length of the wires cannot be shorter than $|L-d|$. For small deviations from

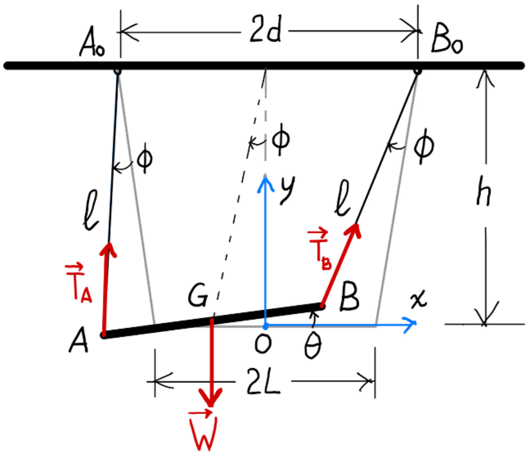

Figure 1. Geometrical configuration and force diagram of the doubly suspended pendulum AB oscillating in the xy-plane for the case $d > L$. An analogous scheme applies to the case $d < L$. The bar and the wires in their equilibrium position are shown in grey.

equilibrium, characterised by the angle ϕ between the wires and the vertical, it is easy to show that θ and ϕ are linearly related:

$$\theta \approx \frac{L-d}{L}\phi. \tag{3}$$

This implies that the positions of points A, B, and the centre G can be expressed as functions of ϕ. Note that $d = L$ is a limiting case: the bar does not rotate about its centre, so θ becomes identically zero, though ϕ remains finite. It is also worth noting that, depending on the sign of $L - d$, the two angles vary in opposite directions, as will be further discussed and illustrated below. We show now that, under the small-angle approximation, the vertical position of the centre G remains nearly constant, $y_G \approx 0$, while the horizontal displacement varies linearly with ϕ, namely $x_G \approx h\phi$, as also seen in figure 1. This can be explicitly derived by considering the vectors from the suspension points to the bar's ends:

$$\begin{aligned} \vec{r}_{\mathrm{AA_0}} &\cong (x_G + d - L, y_G - L\theta - h) \\ \vec{r}_{\mathrm{BB_0}} &\cong (x_G - d + L, y_G + L\theta - h); \end{aligned} \tag{4}$$

requiring these vectors to have length l, and expanding to first order, yields:

$$\begin{aligned} x_G\,(L-d) + y_G h - hL\theta &\cong 0 \\ x_G\,(L-d) - y_G h - hL\theta &\cong 0; \end{aligned} \tag{5}$$

summing and subtracting these relations one finds, as expected,

$$x_G \approx h\frac{L}{L-d}\theta = h\phi, \quad y_G \approx 0. \tag{6}$$

Therefore, the most convenient and unique coordinate to describe the system is the angle ϕ. This becomes even clearer when analysing the system's dynamics, i.e. by formulating and solving the Newtonian cardinal equations of motion in the following form:

$$\begin{aligned} m\vec{a}_G &= \vec{W} + \vec{T}_A + \vec{T}_B \\ I_G \frac{\mathrm{d}^2\vec{\theta}}{\mathrm{d}t^2} &= \vec{\tau}_G = \vec{r}_A \times \vec{T}_A + \vec{r}_B \times \vec{T}_B \end{aligned} \quad . \tag{7}$$

Here, we introduce the acceleration $\vec{a}_G$ of the centre of mass, the weight of the bar $\vec{W} = m\vec{g}$ and the tensions in the wires $\vec{T}_A$, $\vec{T}_B$ which act at the endpoints A and B of the bar, as illustrated again in figure 1. Both equations can now be projected onto the Cartesian reference frame and reformulated using the angle ϕ instead of θ, which, as previously noted, becomes meaningless in the case $d = L$. We also introduce the moment of inertia I_G of the bar with respect to rotations about its centre of mass. Consequently, $I_G = m(L/2)^2/12 = mL^2/3$. Projection is straightforward by using the wires' directions (4) to express the components of the forces. The result is

$$\begin{aligned} m\ddot{x}_G = mh\ddot{\phi} = T_{A_x} + T_{B_x} &\approx (T_A - T_B)\left(\frac{L-d}{l}\right) - (T_A + T_B)\frac{h\phi}{l} \\ m\ddot{y}_G = 0 = T_{A_y} + T_{B_y} - mg &\approx (T_A - T_B)\left(\frac{L-d}{l}\right)\phi + (T_A + T_B)\frac{h}{l}. \end{aligned} \tag{8}$$

The rotational cardinal equation can be projected along the axis perpendicular to the plane xy. At this aim, the external product defining the torque generated by the wire tensions about the centre of mass is computed again in the small angle, linear approximation and the result is

$$I_G\ddot{\theta} = \frac{1}{3}mL^2\frac{L-d}{L}\ddot{\phi} \approx -\frac{Lh}{l}(T_A - T_B) - \frac{d}{l}(L-d)(T_A + T_B)\phi. \quad (9)$$

Expressions (8) and (9) constitute an algebraic, linear system of equations which can be solved to give a relation between $\ddot{\phi}$ and ϕ as well as expressions for T_{A} and T_{B} which are the following:

$$\ddot{\phi} \approx -\frac{g}{l_{\mathrm{eff}}}\phi, \quad l_{\mathrm{eff}} = \frac{hL}{3}\frac{3l^2 - 2(L-d)^2}{l^2L - (L-d)^3} \quad (10)$$

and

$$T_{\mathrm{A,B}} \approx \frac{mg}{2}\frac{l}{h}\left[1 \pm \frac{h\phi}{L}\frac{(L-d)(L-3d)}{3l^2 - 2(L-d)^2}\right]. \quad (11)$$

The most important result here, as expected, is that—looking at equation (10)—the system undergoes harmonic motion, in the small angle approximation, with angular frequency $\omega = \sqrt{g/l_{\mathrm{eff}}}$. As a first consequence, we obtain the time dependence not only of the oscillation angle ϕ but also—according to equation (6)—of the rotational angle θ of the bar respect to its horizontal equilibrium alignment, as well as of the x_{G} coordinate of the centre of mass:

$$\phi(t) = \phi_0\cos\omega t, \quad \theta(t) = \frac{L-d}{L}\phi_0\cos\omega t, \quad x_{\mathrm{G}}(t) = h\phi_0\cos\omega t. \quad (12)$$

Moreover, the positions of the endpoints A and B of the bar evolve in time according to

$$\vec{r}_{\mathrm{A}}(t) \approx (h\phi(t) - L, (d-L)\phi(t)),$$
$$\vec{r}_{\mathrm{B}}(t) \approx (h\phi(t) + L, (L-d)\phi(t)). \quad (13)$$

These expressions imply that, once again only in the small angle approximation, the endpoints of the bar seem to follow rectilinear trajectories, with slopes $\pm(d-L)/h$ for points A and B, respectively. We finally observe that in the critical configuration where $d = L$, i.e. when the two wires are constantly parallel, the bar does not rotate about its centre of mass during the oscillation, as previously anticipated. This is also clearly shown by the motion of the endpoints A and B, which seem to undergo pure translation. The corresponding effective length of the system becomes simply $l_{\mathrm{eff}} = l$, as expected for a simple pendulum located at the centre of mass G, suspended at a distance l from the pivot point. As a final special case, when $d = 0$—i.e. when the suspension points coincide—the effective length becomes

$$l_{\mathrm{eff}}^{(d=0)} = \frac{3l^2 - 2L^2}{3\sqrt{l^2 - L^2}} = \frac{3l^2 - 2L^2}{3h}. \quad (14)$$

This expression is consistent with the oscillation/rotation of a rigid bar of length L about a pivot located at a distance h from its centre of mass. In this case, the moment of inertia, according to the Steiner–Huygens theorem, is given by:

$$I_O = I_G + mh^2 = mL^2/3 + mh^2 = \frac{m}{3}\left(3l^2 - 2L^2\right). \quad (15)$$

By inserting this form of the momentum of inertia, the oscillation frequency associated with the effective length in equation (14) is readily recovered. In all the cases discussed above, we have assumed that the pendulum is released from the initial angle ϕ_0 with zero initial velocity.

3. Experimental

The pendulum can be constructed in a relatively simple manner. In figure 2, the experimental setup used in this study is shown: metal bars of different lengths (here $2l = 72$ mm and 132 mm were the dimensions of the two chosen bars) can be suspended using two identical nylon wires (here 102 mm for the short bar and 123 mm for the long one). The supporting structure allows adjustment of the distance $2d$ between the suspension points. The wires are attached to the bars via screw–nut assemblies, enabling fine adjustment of their distance from the bar's endpoints.

To acquire data regarding the positions of key elements in the setup (namely, the endpoints and centre of gravity of the bar), the motion was recorded using a smartphone in slow-motion mode (240 fps) to improve time resolution. The resulting videos were analysed using dedicated tracking software; in this study, Vernier video analysis was employed, although other options such as the open-source software *Tracker* are also available [9]. Effective video tracking requires proper lighting and the use of clear, high-contrast markers on the moving object to enhance the visibility of the points to be tracked. A crucial step is the accurate calibration of the spatial scale and reference axes used during the tracking process. These aspects are well documented in the user manuals and tutorials provided with the respective software packages and will not be discussed further here.

Figure 3 shows three tracking sessions corresponding to the cases of interest in this study, namely when the distance between the suspension points is greater than, equal to, or less than the length of the bar. The tracked points are the endpoints A and B, and the centre of mass G. The expected motions are clearly observable: points A and B seem to move along straight-line trajectories with opposite slopes when d is either greater or smaller than L, while they seem to move horizontally when $d = L$. In all cases, the centre of mass moves essentially along a horizontal path. The initial angle ϕ_0 was chosen somewhat arbitrarily, but sufficiently small so that the validity of the small-angle approximation is evident in the observed negligible vertical displacement of the centre of mass, $y_G \approx 0$.

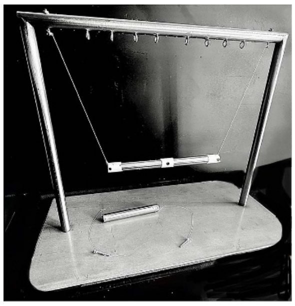

Figure 2. Experimental setup of the doubly suspended pendulum: the long bar has markers attached at its endpoints and at its centre of mass.

Figure 4 provides an alternative visualisation of the pendulum motion, obtained through long-exposure photography (~0.5 s) in complete darkness, using a strobe light emitting six flashes at a repetition rate of 25 Hz. The initial angle in these images was chosen slightly larger than in figure 3 to improve the visual separation of the bar's successive positions. The characteristic motions for $d > L$, $d = L$, and $d < L$ become clearly observable with this technique, which—prior to the advent of high-speed smartphone cameras—was widely and effectively used.

Another key reference quantity is the effective length of the pendulum, or equivalently—by virtue of equation (10)—its oscillation period. This can be readily determined from the tracked motions shown in figure 3. Most tracking software includes a feature for fitting the time dependence of any selected coordinate; by specifying a sine function, the angular frequency or the period is directly extracted. The measured periods for the two bars, plotted in figure 5 as a function of the suspension point distance, demonstrate

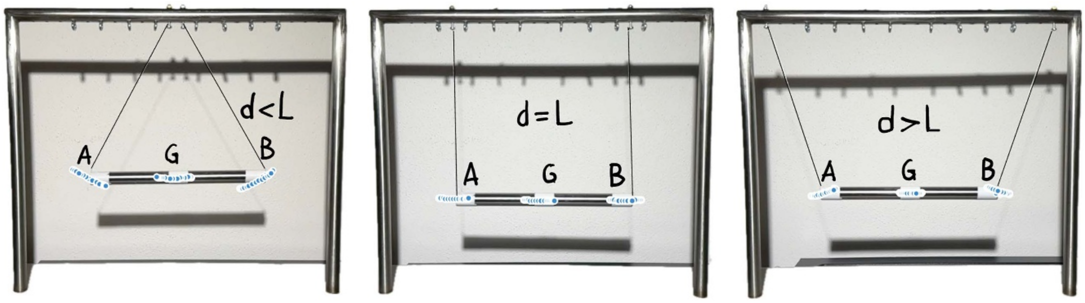

Figure 3. Tracked trajectories of the pendulum for varying suspension point distances. Endpoints move along small circles with different centres for $d < L$ and $d > L$. In the small-angle approximation, the tracked points A, B, and G appear to lie on straight segments with different slopes.

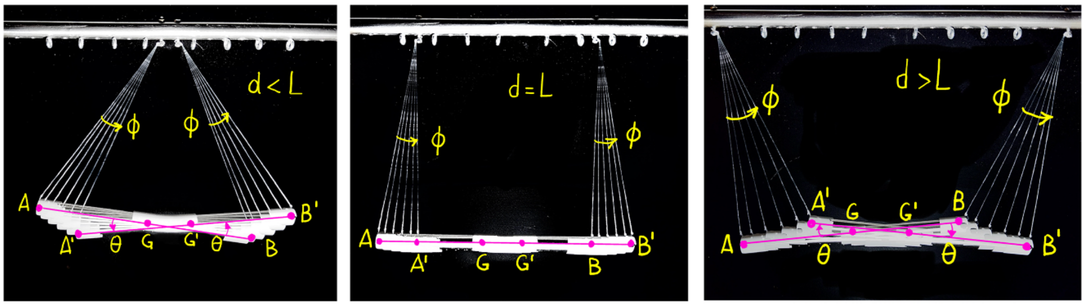

Figure 4. Stroboscopic images of the pendulum motion for different suspension point distance. Notice the different relationships between angles θ and ϕ when $d < L$ and $d > L$. There is no rotation relative the bar's centre of mass for $d = L$. Points A, A$'$; G, G$'$; and B, B$'$ represent the positions of the endpoints and the centre of mass at two different angles of oscillation.

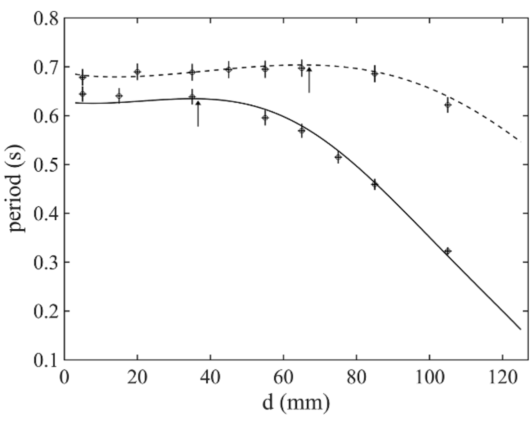

Figure 5. Oscillation period: experimental data (crosses) and theoretical curves (solid: short bar; dashed: long bar). Vertical arrows indicate the cases with $d = L$.

good agreement between theory and experiment. Uncertainties shown in figure 5 are estimated through low-sensitivity error propagation.

4. Conclusions

In this work, we have presented a simple example of a classical mechanical system, which serves as a non-trivial case study for exploring fundamental concepts in mechanics and the approximations they entail. The close agreement between experimental observations and the theoretical Newtonian model supports the validity of linear approximations and underscores the pedagogical value of carefully constructed mechanical analyses—especially for the physical pendulum discussed here, which exhibits oscillatory motion under quite intriguing geometric constraints. This setup has been presented and discussed with a group of about 30 undergraduate physics students attending a first-year classical mechanics course, in order to foster their appreciation of the practical usability of theoretical concepts in a laboratory context (and vice-versa). According to students' feedback, the combination of basic theory, more advanced considerations (in particular, numerical approximation for small angles and the less familiar pendulum setup considered here), and actual measurements—including the always effective experimental tracking and analysis of moving objects—contributes to a more robust and convincing presentation of the topic. While a Lagrangian formulation would certainly have been possible, we opted to highlight the more direct and intuitive insights offered by the Newtonian approach. Moreover, the behaviour of this system can be effectively reproduced using the Algodoo simulation platform, which enables numerical evaluation of kinematic and dynamic variables alongside real-time visualisation of the pendulum's motion [10], thus providing additional support for this activity.

Data availability statement

All data that support the findings of this study are included within the article (and any supplementary files).

Received 12 May 2025, in final form 9 June 2025
Accepted for publication 16 June 2025
https://doi.org/10.1088/1361-6552/ade4ed

References

[1] Gauld C 2004 Pendulums in the physics education literature: a bibliography *Sci. Educ.* **13** 811–32
[2] Baker G L and Blackburn J A 2005 *The Pendulum: A Case Study in Physics* (Oxford University Press)
[3] Then J W 1965 Bifilar pendulum: an experimental study for the advanced laboratory *Am. J. Phys.* **33** 545–7
[4] Then J W and Chiang K 1970 Experimental determination of moments of inertia by the bifilar pendulum method *Am. J. Phys.* **38** 537–9
[5] Hinrichsen P F 2016 In plane oscillation of a bifilar pendulum *Phys. Educ.* **51** 065023–8
[6] Kleppner D and Kolenkow R J 2014 *An Introduction to Mechanics* (Cambridge University Press)
[7] Taylor J R 2005 *Classical Mechanics* (University Science Books)
[8] Bissell J J and Bhamidimarri S K 2020 Introducing the trapezoidal pendulum: dynamics of coupled pendula suitable for distance teaching *Phys. Educ.* **55** 065008–15
[9] Open Source Physics Tracker Video Analysis and Modeling Tool (available at: https://opensourcephysics.github.io/tracker-website/)
[10] Gregorcic B and Bodin M 2017 Algodoo: a tool for encouraging creativity in physics teaching and learning *Phys. Teach.* **55** 25–28

Stefano Oss is a full professor of physics education and history of physics at the Department of Physics, University of Trento, Italy. His work focuses on teacher training, science communication, and research in the teaching of classical mechanics, thermodynamics, and applications of modern physics.